Direct Fabrication of Zero- and One-Dimensional Metal Nanocrystals by Thermally Assisted Electromigration

Jong Min Yuk,[†,‡] Kwanpyo Kim,[§,⊥,∥] Zonghoon Lee,[‡] Masashi Watanabe,[‡,△] A. Zettl,[§,⊥,∥] Tae Whan Kim,[¶] Young Soo No,[¶] Won Kook Choi,[#] and Jeong Yong Lee[†,*]

[†]Department of Materials Science and Engineering, KAIST, Daejeon 305-701, Korea, [‡]National Center for Electron Microscopy, [§]Materials Sciences Division, Lawrence Berkeley National Laboratory, [⊥]Department of Physics and [∥]Center of Integrated Nanomechanical Systems, University of California at Berkeley, California 94720, [¶]National Research Laboratory for Nano Quantum Electronics Laboratory, Department of Electronics and Communications Engineering, Hanyang University, Seoul 133-791, Korea, and [#]Thin Film Materials Research Center, Korea Institute of Science and Technology, Seoul 136-791, Korea. [△]Current address: Department of Materials Science and Engineering, Lehigh University, Bethlehem, Pennsylvania 18015.

ABSTRACT Zero- and one-dimensional metal nanocrystals were successfully fabricated with accurate control in size, shape, and position on semiconductor surfaces by using a novel *in situ* fabrication method of the nanocrystal with a biasing tungsten tip in transmission electron microscopy. The dominant mechanism of nanocrystal formation was identified mainly as local Joule heating-assisted electromigration through the direct observation of formation and growth processes of the nanocrystal. This method was applied to extracting metal atoms with an exceedingly faster growth rate ($\sim 10^5$ atoms/s) from a metal-oxide thin film to form a metal nanocrystal with any desired size and position. By real-time observation of the microstructure and concurrent electrical measurements, it was found that the nanostructure formation can be completely controlled into various shapes such as zero-dimensional nanodots and one-dimensional nanowires/nanorods.

KEYWORDS: nanodots · nanowires · nanorods · nanostructures · *in situ* nanofabrication · scanning probe · metal · Joule heating · electromigration · *in situ* transmission electron microscopy

There is a great interest in the fabrication of zero- (0-D, dot) and one-dimensional (1-D, wire and/or rod) nanocrystals and the design of their size, shape, and position on semiconductor substrates for applications in memories, transistors, and sensors.[1−5] However, direct fabrication of nanocrystals is a great challenge to accurately control their size, shape, and position, which extremely affect the characteristics of single-electron devices because of quantum confinement and surface effects.[6,7]

As potential engineering tools to directly fabricate position-controlled nanocrystals,[8−11] scanning probe techniques such as scanning tunneling microscopy (STM) and atomic force microscopy (AFM) have been intensively employed because single-atom manipulation has been demonstrated.[12−15] However, these techniques have a limit for controlling nanocrystal size and shape because governing mechanisms of nanocrystal formation still remain uncertain. Real-time direct observations required for elucidation of nanocrystal formation mechanisms at atomic scales are hardly achievable in current scanning probe instruments with the serial manner procedure: first prescanning the clean surface, second transporting and manipulating atoms on the surface one at a time, and then finally postscanning manufactured features.[16] Furthermore, these techniques have a principle drawback of repetitive manipulation of individual atoms to fabricate nanocrystals with desired size and shape, which is extremely time-consuming (for example, 120 atoms/9 h).[17] Therefore, a formidable method needs to be developed to both directly form and manipulate desired 0-D and 1-D nanocrystals with fast growth speed in *in situ* observation.

In this study, 0-D and 1-D metal nanocrystals were successfully fabricated with accurate control in size, shape, and position on semiconductor surfaces, accompanied with a much faster growth rate ($\sim 10^5$ atoms/s) than any other conventional scanning probe approaches. The dominant mechanisms of nanocrystal formation were clearly identified as Joule heating and assisted electromigration by using a novel *in situ* fabrication method with a biasing W tip as the scanning probe in transmission electron microscopy (TEM).

RESULTS AND DISCUSSION

For direct observation of the Zn nanocrystal formation/manipulation by the scanning probe technique, in this *in situ* study, a specially designed holder with a biasing

*Address correspondence to j.y.lee@kaist.ac.kr.

Received for review November 23, 2009 and accepted May 06, 2010.

Published online May 13, 2010. 10.1021/nn901674p

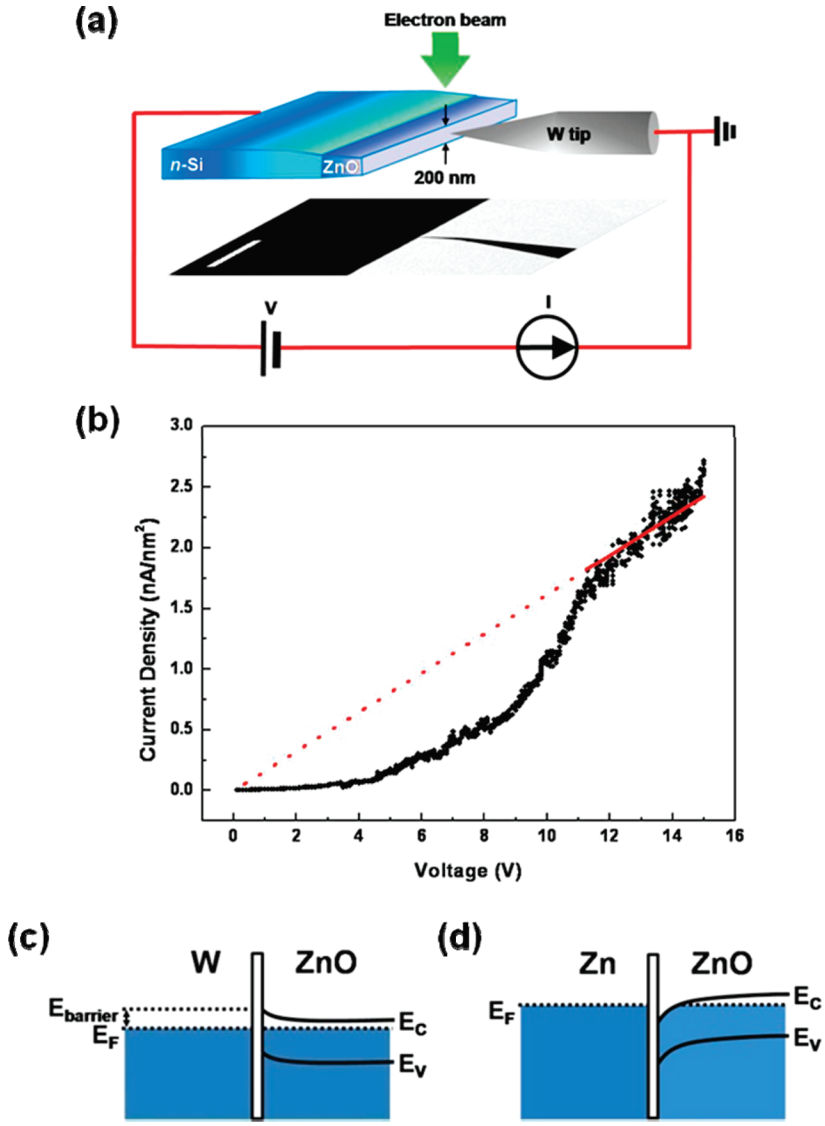

Figure 1. Summary of the current density−voltage measurement at the nanoelectrical contact during *in situ* Zn nanostructure formation. (a) Schematic diagram of the *in situ* nanofabrication experiment in TEM. An actual TEM image of the tip and sample is accompanied. The scale bar represents 20 μm. (b) *J*−*V* characteristic plot during *in situ* nanofabrication for extracting Zn ions from a ZnO thin film. Solid and dashed lines indicate a fitting result to a linear function in the voltage range >11.3 V and an extrapolation to lower voltage region, respectively. (c) Energy band diagram of W/ZnO junction under equilibrium conditions. A Shottky barrier with height $E_{barrier}$ forms in the W side. (d) Ohmic energy band diagram of the Zn/ZnO junction under equilibrium conditions. The energy levels of conduction and valence bands in the ZnO are denoted by E_C and E_V, respectively, and the Fermi level by E_F.

W tip was used in TEM. Positioning of an electrochemically etched fine W tip onto the surface of a cross-sectional ZnO thin film enables metal−semiconductor nanocontact junctions, as shown in Figure 1a.

Through these junctions, we can apply dc voltage and monitor the electrical current. Figure 1b shows a current density−voltage (*J*−*V*) characteristic curve directly measured during the *in situ* experiment. We adjust the tip and sample positions to keep taking images of those areas because there is a lateral drift when the applied bias voltage was changed. The *J*−*V* characteristic curve changes from nonlinear to linear response at a certain applied voltage (current density *J* is the electrical current divided by the contact area of tip with the specimen). This response change can be attributed to the formation of Zn nanocrystal at the junctions. Since the work function of W is 4.55 eV and the work function and electron affinity of ZnO are 4.45 and 4.29 eV,[18,19] respectively, a Schottky barrier is formed at the contact junction between W and ZnO, as illustrated in Figure 1c. The nonlinear behavior in the *J*−*V* curve can be explained as a surface breakdown. When the current density reaches the critical value J_T, electromigration of Zn ions occurs and a Zn nanodot is formed. Since the work function of Zn is 3.63 eV,[18] there is no energy barrier at the Zn/ZnO interface; thus, the contact between Zn and ZnO is likely to be Ohmic, as shown in Figure 1d, and the *J*−*V* curve becomes linear. From Figure 1b, the J_T value can be estimated as ~1.73 nA/nm^2.

We can facilitate the Zn nanodot fabrication process with a modified method, by establishing the contact with an accordingly bias-maintained W tip, instead of increasing applied bias voltage after the junction formation, as shown in Figure 2. Once the biasing tip is physically contacted with the ZnO surface, a Zn nanodot is grown by electromigration of positive Zn ions to the negatively biased tip (see Supporting Information, movie S1), which occurs rapidly within 0.25 s of a limit of typical electrical recording time. Because electromigration is a very slow process except at higher temperature,[20] this fast Zn nanodot growth indicates that the electromigration process can be accelerated by local Joule heating in the vicinity of the tip-specimen contact. For the electromigration phenomena,[21] the force (F) is typically given as a sum of the electrostatic "direct force", F_d, and the electron mediated "wind force", F_w:

$$F = F_d + F_w = eZ_dE + eZ_wE = e\rho Z_dJ + e\rho Z_wJ \quad (1)$$

where E is the electric field, Z_d and Z_w are the effective valences for the direct and the wind force mediated processes, respectively, and ρ is the electrical resistivity. The direct force is presented if there are charged particles (with an effective charge Z_d) or an accumulation of charge near the particle due to the scattering of current carriers. For self-diffusion in semiconductors,[21] Z_d may be dominant over Z_w. In this experiment, the Zn ions act as electron donors (which results in $Z_d > 0$), and this positive Z_d would lead migration of the Zn ions in the electric field direction along ZnO surfaces, grain boundaries, and Zn interstitial sites. Such migrated Zn ions were condensed at the end of the tip, and the remaining oxygen ions were evaporated as oxygen gas in TEM.

When the biasing tip was withdrawn, a single Zn nanocrystal (nanodot) was created, which was identified by high-resolution TEM imaging and electron diffraction (see Supporting Information, Figure S1). In addition, the created nanodot can be moved to another region on the ZnO surface or dissociated by attaching it to the tip with same magnitudes of the positive bias to induce a molten Zn/ZnO interface as that applied to the ZnO surface to form Zn nanocrystals.

Precise volume control of Zn nanodots was also possible at any designated locations on the surface, as shown in Figure 3a, because both the extracted amount and moving direction of Zn ions strongly depend on the external electrical drive as expressed in eq 1. Multiple contacts with the biasing tip were performed repeatedly and readily on the surface of ZnO thin film by controlling the tip position and distance with *in situ* TEM observation. This contact method enables extraction of metal ions from oxide films in a highly reproducible manner in comparison with any other conventional noncontact approach, where reproduction rates are relatively limited.[22]

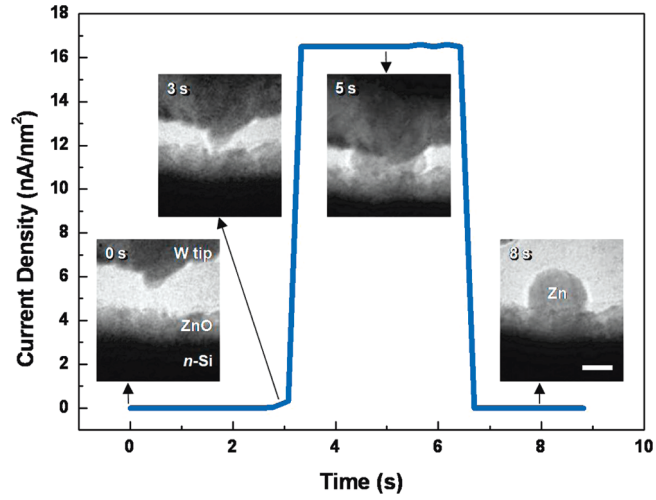

Figure 2. *In situ* creation of a Zn nanodot. J characteristics plotted as a function of the processing time, recorded during the *in situ* Zn nanodot formation. Inserted four video captured TEM images show a sequence of the *in situ* Zn nanodot formation from the ZnO thin film. While the tip is contacted with the ZnO surface, the tunneling current is constant at ~16.5 nA/nm², which is much greater than J_T for extracting Zn ions from the ZnO thin film. The scale bar represents 10 nm.

Figure 3b exhibits how the Zn nanodots grow on the ZnO thin film as a function of J. The volume of Zn nanodots was controlled from 1592 ± 122 to 3123 ± 104 nm³ by electromigration force depending on the current density at the tip with extracting speed of ~10⁵

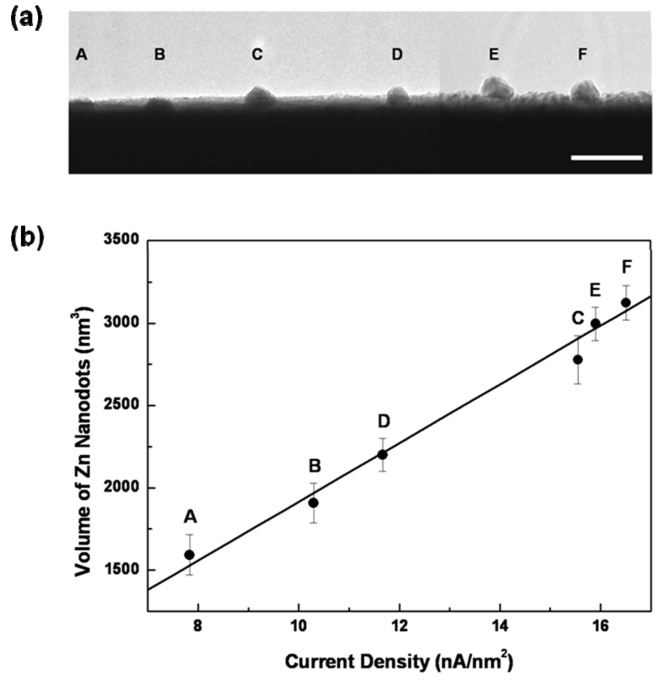

Figure 3. Volume-controlled Zn nanodots created on designated locations. (a) TEM image of an array of six Zn nanodots (A−F) fabricated sequentially. The shapes of A and B are hemispheres, and those of C−F nanodots are spheres. Two different bright-field TEM images including A−D and E and F nanodots are combined because of the TEM image capturing problem. The scale bar represents 50 nm. (b) Volume of Zn nanodots as a function of J. The line represents a fitting result to a linear function.

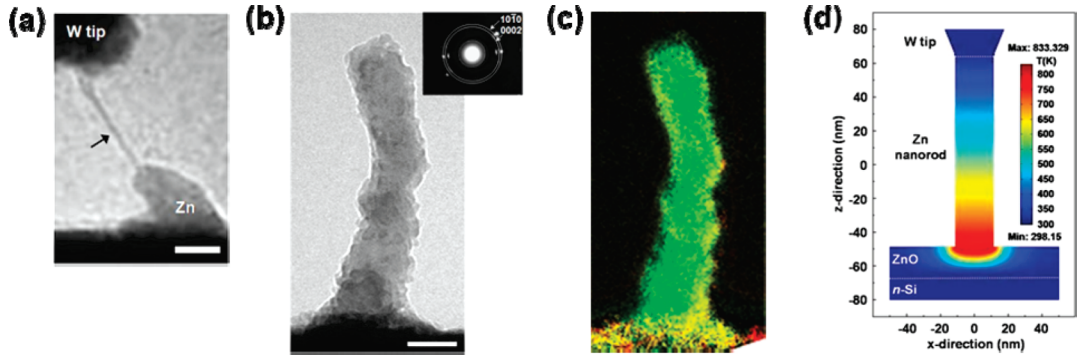

Figure 4. *In situ* fabrication of 1-D Zn nanocrystals. (a) Video captured image of a Zn nanowire in TEM. When the tip was pulled with the withdrawing rate of ~4.5 nm/s, a nanowire indicated by arrow was formed. (b) Bright-field TEM image of another Zn nanorod, which was formed with the withdrawing rate of ~0.7 nm/s. The inserted selected area electron diffraction pattern shows {10$\bar{1}$0} and {0002} planes of hexagonal Zn. The scale bars in (a) and (b) represent 20 nm. (c) Energy-filtered TEM image acquired by using a three-window method at Zn $L_{2,3}$ (green), O K (yellow), and Si L (red) edges. (d) Result of FEM simulation showing temperature gradient from the biasing tip through the Zn nanorod to ZnO thin film.

atoms/s. The linear dependence of the Zn volume against J shown as a fitted line in Figure 3b represents that the Zn volume can be controlled by ~180 nm^3 with an increment of 1 nA/nm^2 in J. Therefore, within the detectable range of the present *in situ* experiment, Zn ions can be extracted from the ZnO thin film until a preselected nanodot size is achieved above J_T. From this linear relationship, the initial Zn volume can be estimated as ~440 nm^3 by extrapolation.

Furthermore, in the same fabrication conditions for 0-D Zn nanodots, 1-D Zn nanowires and nanorods could also be fabricated by controlling the dragging speed of the tip perpendicular to the ZnO surface, as shown in Figure 4a,b (see Supporting Information, movies S2 and S3). These fabrications directly exhibit that it is possible for the electromigration to continuosly extract the Zn ions from the ZnO thin film in the bias duration. It was confirmed that the nanorod consists of pure Zn by energy-filtered TEM, as shown in Figure 4c.

The sufficiently high atomic mobility and driving force (*i.e.*, current density for electromigration) are required to apply the electromigration phenomenon to the nanostructure fabrication in practice. The atomic mobility is strongly influenced by the local temperature T, which can be enhanced due to Joule heating after the Ohmic contact is established. Therefore, in practice, electromigration-induced nanostructure formation can be enhanced by controlling the local temperature.[23]

To determine the temperature gradient from the biasing tip through the Zn nanorod to the ZnO thin film, finite element modeling (FEM) simulation was employed to solve a heat-transport equation in this fabrication condition for the Zn nanorod. The simulation result is shown in Figure 4d. Since the electrical resistivity of ZnO (4.50×10^{-2} Ω m)[24] is much higher than that of Zn (6.01×10^{-8} Ω m)[18] at 298 K, T could be increased up to ~833 K by the Joule heating in a narrow region, where the Zn nanorod is fully contacted with the ZnO thin film. The FEM result indicates that the local temperature can be elevated higher than the Zn melting point in bulk (692 K) at the contact part of the tip with the Zn nanorod due to the Joule heating. The phase transformation of the Zn from liquid to solid status was observed as contrast modification in simultaneous TEM imaging with the Zn formation (see Supporting Information, movie S3). If the local temperature of the molten region of the nanorod is lower than the Zn melting temperature by departing from the Zn/ZnO interface due to the tip manipulation, the molten part is crystallized (see Supporting Information, Figure S2).

This nanofabrication method can be applied to other metallic nanostructure fabrications from metal or metallic compound systems if the thermally assisted electromigration is triggered in combination with the applied current density with elevated local temperature. In other material systems, electromigration direction of metal ions should be considered because dominant force between direct and wind forces is different in every material. In the case of fabricating a metallic nanostructure from metal systems, higher current density than that for semiconductor systems is essential because metals can dissipate enormous power densities without melting.

CONCLUSIONS

In summary, the present study indicates that the mechanism of metallic nanostructure fabrication by the biasing probe is a thermally assisted electromigration. Utilizing this mechanism, the practically rapid nanostructure fabrication was demonstrated to create 0-D Zn nanodots with desired sizes at designated locations by extracting Zn ions from ZnO thin films. Further manipulation enables fabrication of 1-D Zn nanowires and nanorods, as well. The method and condition demonstrated here can be applied in STM and AFM for creating a diverse range of artificial two-dimensional nanostructures, which are constructed by arraying 0-D and 1-D nanocrystals, as templates for the implementation of nanoscale devices.

METHODS

Specimen Preparations and *In Situ* TEM Experiments. ZnO thin films with a thickness of ~20 nm were deposited on *n*-Si (001) substrates by radio frequency magnetron sputtering. The detailed growth procedure of the ZnO thin film deposition is described elsewhere.[25] For the formation of pure metal Zn nanocrystals, ZnO was chosen as a base material because of its relative stiffness, in contrast to other metallic and organic materials. Additionally, it has an excellent thermal stability and resistance against chemical degradation and oxidation.[26] Therefore, the synthesized nanocrystals do not react with the ZnO thin film. Cross-sectional TEM specimens for *in situ* experiments were prepared by cutting with a diamond saw, polishing with diamond films, dimpling to a thickness of ~10 μm, and then final Ar-ion thinning at a liquid nitrogen temperature. The *in situ* experiments were performed in a JEM-2010 LaB_6 instrument (JEOL Ltd.), equipped with a piezo-driven nanomanipulation stage (Nanofactory Instruments AB). We use the acceleration voltage of 100 kV to reduce irradiation damage on the specimen. In TEM, the specimen was approached with an electrochemically etched W tip mounted on the nanomanipulator side, and physical contact was made between the tip and the surface of the ZnO thin films. By applying a bias voltage at the tip, an electrical circuit is established in the holder including the ZnO specimen. The W tip was changed to a clean one whenever the tip was severely contaminated. Moreover, contaminated tips could be cleaned by field-induced dissociation of Zn from the tips. The nanofabrication process was recorded using real-time TEM video imaging with electrical data, which were recorded with ~4 Hz acquisition speed.

FEM Simulation of Temperature Gradient. It is supposed that the Zn nanorod as a one-dimensional system with length L obeys the classical heat equation with Joule heating:

$$\nabla(\kappa\nabla T) + \sigma V^2/L^2 = 0 \qquad (2)$$

where κ is the temperature-dependent thermal conductivity, T the temperature, σ the temperature-dependent electric conductivity, and V the applied voltage across the nanorod. The temperature-dependent parameters of $\kappa(T)$ and $\sigma(T)$ of Zn[27,28] and ZnO[29,30] are well-known. Equation 2 was solved by applying FEM to the entire system with appropriate boundary conditions at a given applied bias of 30 V.[31] Full contact was assumed at both the tip/nanorod and ZnO/nanorod interfaces for this FEM simulation.

Acknowledgment. We thank Mr. Swannee J. Shin at University of California, Berkeley, for discussions. Portions of the present study were performed at the National Center for Electron Microscopy, Lawrence Berkeley National Laboratory, which is supported by the U.S. Department of Energy under Contract No. DE-AC02-05CH11231. J.M.Y. acknowledges the financial support by Priority Research Centers Program through the National Research Foundation of Korea (NRF) funded by the Ministry of Education, Science and Technology (2009-0094040). T.W.K. and Y.S.N. acknowledge the financial support by the Korea Science and Engineering Foundation (KOSEF) grant funded by the Korea government (MEST) (No. R0A-2007-000-20044-0). A.Z. and K.K. acknowledge the financial support by the Director, Office of Energy Research, Office of Basic Energy Sciences, Materials Sciences and Engineering Division, of the U.S. Department of Energy under Contract No. DE-AC02-05CH11231. K.K. received further support from a Samsung Scholarship.

Supporting Information Available: High-resolution TEM image and selected area electron diffraction pattern of Zn single nanocrystal, selected area electron diffraction pattern showing transformation of Zn from liquid into solid, and three videos of the *in situ* fabrication process of Zn nanodot, nanowire, and nanorod. This material is available free of charge *via* the Internet at http://pubs.acs.org.

REFERENCES AND NOTES

1. Averin, D. V.; Likharev, K. K. *Mesoscopic Phenomena in Solids*Altshuler, B. L., Lee, P. A., Webb, R. A., Eds.; Elsevier: Amsterdam, 1991; pp 173−271.
2. Guo, L.; Leobandung, E.; Chou, S. Y. A Silicon Single-Electron Transistor Memory Operating at Room Temperature. *Science* **1997**, *275*, 649–651.
3. Klein, D. L.; Roth, R.; Lim, A. K. L.; Alivisatos, A. P.; McEuen, P. L. A Single-Electron Transistor Made from a Cadmium Selenide Nanocrystal. *Nature* **1997**, *389*, 699–701.
4. Likharev, K. K. Single-Electron Devices and Their Applications. *Proc. IEEE* **1999**, *87*, 606–632.
5. Ray, V.; Subramanian, R.; Bhadrachalam, P.; Ma, L. C.; Kim, C. U.; Koh, S. J. CMOS-Compatible Fabrication of Room-Temperature Single-Electron Devices. *Nat. Nanotechnol.* **2008**, *3*, 603–608.
6. Heitmann, J.; Müller, F.; Zacharias, M.; Gösele, U. Silicon Nanocrystals: Size Matters. *Adv. Mater.* **2005**, *17*, 795–803.
7. Yang, D. S.; LaO, C.; Zewail, A. H. 4D Electron Diffraction Reveals Correlated Unidirectional Behavior in Zinc Oxide Nanowires. *Science* **2008**, *321*, 1660–1664.
8. Crommie, M. F.; Lutz, C. P.; Eigler, D. M. Confinement of Electrons to Quantum Corrals on a Metal Surface. *Science* **1993**, *262*, 218–220.
9. Nilius, N.; Wallis, T. M.; Ho, W. Development of One Dimensional Band Structure in Artificial Gold Chains. *Science* **2002**, *297*, 1853–1856.
10. Heinrich, A. J.; Lutz, C. P.; Gupta, J. A.; Eigler, D. M. Molecule Cascades. *Science* **2002**, *298*, 1381–1387.
11. Hirjibehedin, C. F.; Lutz, C. P.; Heinrich, A. J. Spin Coupling in Engineered Atomic Structures. *Science* **2006**, *312*, 1021–1024.
12. Eigler, D. M.; Schweizer, E. K. Positioning Single Atoms with a Scanning Tunnelling Microscope. *Nature* **1990**, *344*, 524–526.
13. Eigler, D. M.; Lutz, C. P.; Rudge, W. E. An Atomic Switch Realized with the Scanning Tunnelling Microscope. *Nature* **1991**, *352*, 600–603.
14. Whitman, L. J.; Stroscio, J. A.; Dragoset, R. A.; Celotta, R. J. Manipulation of Adsorbed Atoms and Creation of New Structures on Room-Temperature Surfaces with a Scanning Tunneling Microscope. *Science* **1991**, *251*, 1206–1210.
15. Stroscio, J. A.; Tavazza, F.; Crain, J. N.; Celotta, R. J.; Chaka, A. M. Electronically Induced Atom Motion in Engineered $CoCu_n$ Nanostructures. *Science* **2006**, *313*, 948–951.
16. Sincell, M. NanoManipulator Lets Chemists Go Mano a Mano with Molecules. *Science* **2000**, *290*, 1530.
17. Sugimoto, Y.; Abe, M.; Hirayama, S.; Oyabu, N.; Custance, Ó.; Morita, S. Atom Inlays Performed at Room Temperature Using Atomic Force Microscopy. *Nat. Mater.* **2005**, *4*, 156–159.
18. Lide, D. R., Ed. *CRC Handbook of Chemistry and Physics*, 89th ed.; CRC Press: New York, 2009.
19. Hossain, F. M.; Nishii, J.; Takagi, S.; Ohtomo, A.; Fukumura, T.; Fujioka, H.; Ohno, H.; Koinuma, H.; Kawasaki, M. Modeling and Simulation of Polycrystalline ZnO Thin-Film Transistors. *J. Appl. Phys.* **2003**, *94*, 7768–7777.
20. Sorbello, R. S. Theory of Electromigration. *Solid State Phys.* **1998**, *51*, 159–231.
21. Svensson, K.; Olin, H.; Olsson, E. Nanopipettes for Metal Transport. *Phys. Rev. Lett.* **2004**, *93*, 145901.
22. Salling, C. T.; Lagally, M. G. Fabrication of Atomic-Scale Structures on Si(001) Surfaces. *Science* **1994**, *265*, 502–506.
23. Trouwborst, M. L.; van der Molen, S. J.; van Wees, B. J. The Role of Joule Heating in the Formation of Nanogaps by Electromigration. *J. Appl. Phys.* **2006**, *99*, 114316.
24. Carcia, P. F.; McLean, R. S.; Reilly, M. H.; Nunes, G., Jr. Transparent ZnO Thin-Film Transistor Fabricated by RF Magnetron Sputtering. *Appl. Phys. Lett.* **2003**, *82*, 1117–1119.
25. Shin, J. W.; Lee, J. Y.; Kim, T. W.; No, Y. S.; Cho, W. J.; Choi, W. K. Growth Mechanism of Thin-Film Columnar Structures in Zinc Oxide on p-Type Silicon Substrates. *Appl. Phys. Lett.* **2006**, *88*, 091911.
26. Segawa, Y.; Ohtomo, A.; Kawasaki, M.; Koinuma, H.; Tang, Z. K.; Yu, P.; Wong, G. K. L. Growth of ZnO Thin Film by Laser MBE: Lasing of Exciton at Room Temperature. *Phys. Status Solidi (b)* **1997**, *202*, 669–672.

27. Ho, C. Y.; Powell, R. W.; Liley, P. E. Thermal Conductivity of the Elements. *J. Phys. Chem. Ref. Data* **1972**, *1*, 279–421.
28. McBride, B. J.; Gordon, S.; Reno, M. A. Thermodynamic Data for Fifty Elements. *NASA Technical Paper* **1993**, 3287.
29. Kingery, W. D.; Francl, J.; Coble, R. L.; Vasilos, T. Thermal Conductivity: X, Data for Several Pure Oxide Materials Corrected to Zero Porosity. *J. Am. Ceram. Soc.* **1954**, *37*, 107–110.
30. Pankratz, L. B. Thermodynamic Data of Elements and Oxides. *U.S. Bur. Mines Bull.* **1982**, *672*, 509.
31. Begtrup, G. E.; Ray, K. G.; Kessler, B. M.; Yuzvinsky, T. D.; Garcia, H.; Zettl, A. Probing Nanoscale Solids at Thermal Extremes. *Phys. Rev. Lett.* **2007**, *99*, 155901.